Using light and heat to controllably switch and reset disorder configuration in nanoscale devices

A. M. See, A. R. Hamilton, and A. P. Micolich*
School of Physics, University of New South Wales, Sydney NSW 2052, Australia

M. Aagesen and P. E. Lindelof
Nanoscience Center, University of Copenhagen, Universitetsparken 5, DK-2100 Copenhagen, Denmark
(Received 11 August 2014; revised manuscript received 28 January 2015; published 19 February 2015)

Quantum dots exhibit reproducible conductance fluctuations at low temperatures due to electron quantum interference. These fluctuations are not solely determined by dot geometry; they are also highly sensitive to the underlying disorder potential. Here we exploit this sensitivity to better understand the role that background impurities play in the electronic properties of undoped AlGaAs/GaAs heterostructures, and nanoscale devices based thereon. In particular, we report the remarkable ability to first alter the disorder potential in an undoped AlGaAs/GaAs heterostructure by optical illumination and then reset it back to its initial configuration by room temperature thermal cycling in the dark. We attribute this behavior to a mixture of C background impurities acting as shallow acceptors and deep trapping by Si background donor impurities, i.e., DX centers. This "alter and reset" capability is not possible in modulation-doped heterostructures and offers a route to new studies of how background impurities influence transport in nanoscale semiconductor devices.

DOI: 10.1103/PhysRevB.91.085417 PACS number(s): 73.23.Ad, 72.10.−d, 71.55.Eq

Disorder is an important issue in nanoelectronics; as a device is reduced in size it becomes more sensitive to temporal fluctuations and spatial inhomogeneities in the charged impurity distribution [1]. The temporal fluctuations cause decoherence [2,3], noise [4], and device irreproducibility [5,6]. These are troublesome for the development of quantum applications for semiconductor devices. Spatial inhomogeneities interrupt electron flow [7] adversely affecting [8] practical realization of concepts such as topological quantum computation using the $\frac{5}{2}$ fractional quantum Hall state [9]. These barriers to applications have fueled research to reduce, control, and better understand disorder in nanoscale electronic devices.

Approaches to disorder reduction for nanoscale devices include modulation doping [10], short period superlattice doping [11,12], and undoped heterostructures where the carriers are induced using either a metal [13,14] or degenerately-doped semiconductor gate [15,16]. While modulation-doped structures still provide the highest mobilities, undoped heterostructures provide two distinct advantages. First, short range neutral disorder dominates over long range Coulombic disorder. This brings benefits such as enhanced robustness of the $\frac{5}{2}$ fractional quantum Hall state [8], and improved experimental access to the metallic state generated by electron-electron interactions in 2D systems [17]. Second, the absence of intentional ionized impurities gives electrical properties that are remarkably robust to thermal cycling [18], in stark contrast to modulation-doped heterostructures [6]. Both features demonstrate there is much more to disorder than the popular metric of mobility alone [19]. They also strongly motivate the quest for a deeper understanding of the nature of disorder in undoped AlGaAs/GaAs heterostructure devices.

Quantum interference provides an interesting route to studying disorder in nanoscale devices. A quantum dot's low temperature magnetoconductance shows quantum interference fluctuations that are highly sensitive to the paths electrons take in traversing the device [20]. These "magnetoconductance fluctuations" (MCF) are influenced by both the dot geometry [21] and the underlying disorder potential [19,22] in dots smaller than the large-angle scattering length, i.e., in the "ballistic" transport regime. If the dot geometry is fixed, changes in the MCF can be used to probe the physics of dopants, e.g., the intentional Si donors [6] and acceptors [23], within the device. The underlying physics is very similar to that reported in studies of universal conductance fluctuations [24] (UCF) in Si MOSFETs [25,26], AlGaAs/GaAs quantum wires [27] and metal films [28] in the 1980s, but has only recently been applied to "ballistic" quantum dots [6]. We recently made a remarkable finding—the MCF becomes highly reproducible, even after thermal cycling to room temperature, if the intentional dopants are removed, i.e., the quantum dot is made using an undoped heterostructure [18]. This result naturally leads to interesting questions: An undoped heterostructure is never 100% pure, so what role does the low density of nonintentional "background" impurities inevitably incorporated into the heterostructure during growth play? Since these impurities are "invisible" thermally, can we probe them another way, for example, optically? Might it be possible to use this small density of impurities as a new way to control electrical properties towards novel applications?

Here we demonstrate the ability to alter the disorder potential in undoped heterostructures by optical illumination, detect the resulting changes via the low temperature magnetoconductance, and then reset the disorder potential back to its initial configuration by thermally cycling the device to room temperature. This remarkable capability, not possible in conventional modulation-doped heterostructures [6], provides the opportunity to better understand how even small densities of charged background impurities influences transport in nanoscale devices. Note that the technique could be readily extended towards understanding background disorder in materials beyond III-V semiconductors, e.g., graphene [29,30]. One only needs a quantum dot showing quantum interference fluctuations.

*adam.micolich@nanoelectronics.physics.unsw.edu.au

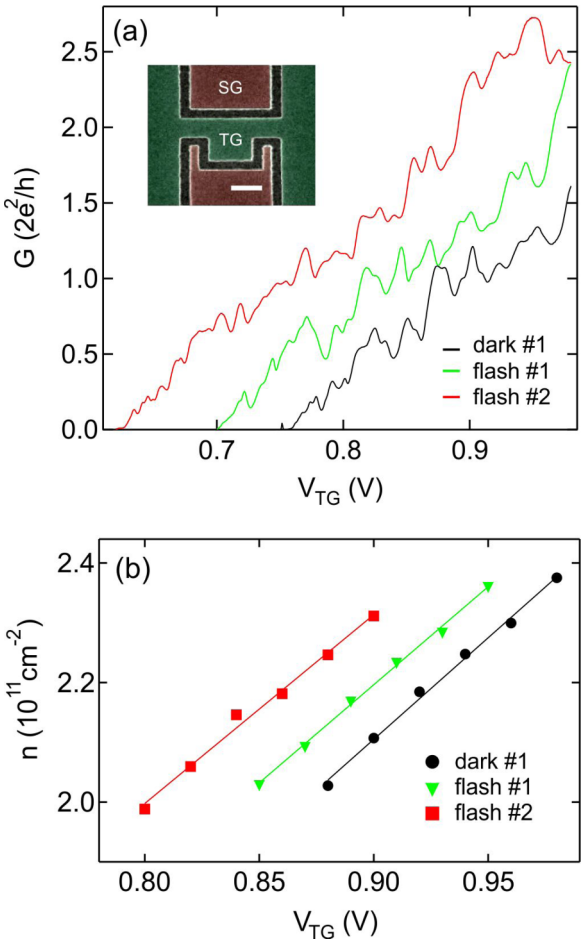

FIG. 1. (Color online) (a) A comparison of dot conductance G vs top-gate voltage V_{TG} obtained at temperature $T = 250$ mK and side-gate voltage $V_{SG} = 0$. (Inset) Scanning electron micrograph of the device; the scale bar represents 500 nm. (b) Two-dimensional electron density n vs V_{TG} for different amounts of illumination. The straight lines are fits to the experimental data.

A scanning electron micrograph of our device is shown in the inset to Fig. 1(a). It was made using a heterostructure consisting of an undoped GaAs substrate overgrown with 160 nm undoped $Al_{0.33}Ga_{0.67}As$, 25 nm undoped GaAs, and a 35 nm n^+ GaAs cap, which remains highly conductive at low temperature. The cap is divided into three independent gates—a top-gate (green) and two side-gates (red)—using electron-beam lithography and shallow wet etching. The NiGeAu ohmic contacts are produced using an established self-aligned process [16,31]. The dot and the 2D electron gas (2DEG) source and drain reservoirs are populated electrostatically when the top gate (TG) is biased to a sufficiently positive voltage V_{TG}. The width of the quantum point contacts (QPCs) connecting the dot to source and drain can be tuned via a negative voltage V_{SG} applied to the side gates (SG). Electrical characterization of a Hall bar made using the same heterostructure at 4.2 K gave a mobility $\mu \sim 300{,}000$ cm^2/Vs at $n \sim 1.8 \times 10^{11}$ cm^{-2}, corresponding to $\ell \sim 2.1$ μm, which is larger than the dot dimensions (760 × 660 nm). Electrical measurements were performed at temperature $T \approx 250$ mK using a pumped ^{3}He cryostat (Oxford Instruments Heliox), with the magnetoconductance $G(B)$ obtained by standard four-terminal lock-in techniques using a fixed 100 μV excitation voltage at a frequency of 11 Hz. The variable magnetic field B was applied along the heterostructure growth direction [perpendicular to the plane of Fig. 1(a) inset]. Illumination was performed using a red light-emitting diode (LED) mounted in close proximity to the device. The illuminated area is several mm in diameter, encompassing the entire active region of the device. Within this illuminated area the power density is 1mW/m^2. Illumination is implemented via a control box that drives an LED current of 1 mA for a single 100 ms pulse (see Fig. S1 of Ref. [32] for the emission spectrum of this LED). Further details on the undoped devices and electrical measurements are available elsewhere [16,18,31].

Figure 1(a) shows traces of zero field conductance $G(B = 0)$ versus V_{TG} obtained in a single cooldown: before illumination denoted "dark #1" (black), after a 100 ms illumination denoted "flash #1" (green), and after another 100 ms illumination denoted "flash #2" (red). In each case G increases as V_{TG} is made more positive, reflecting a gate-induced accumulation of electrons in the dot and source/drain contacts. The threshold voltage V_{th}—defined here as the lowest V_{TG} where G becomes nonzero—decreases from 0.76 V to 0.7 V and then 0.62 V after the first and second illuminations, respectively. This V_{th} shift indicates the optical ionization of background impurities and a commensurate increase in electron density. To more clearly demonstrate the density increase in Fig. 1(b) we plot the electron density n from Shubnikov-de Haas measurements of an adjacent Hall-bar segment on this device versus V_{TG}; the black circles, green triangles, and red squares are data obtained before, between, and after the two illuminations, respectively. With each illumination, the density increases by 4–5%. This density increase is persistent, as previously shown in an inverted, undoped AlGaAs/GaAs heterointerface [33]. The slope of n versus V_{TG} in Fig. 1(b) is constant, demonstrating that illumination does not alter the gate-2DEG capacitance.

The fluctuations in the gate sweeps in Fig. 1(a) arise from quantum interference [34] and represent a "fingerprint" of transport through the dot similar to $G(B)$. The exact fluctuation pattern varies with each illumination due to a change in the disorder potential within the dot. We can assess this further using $G(B)$ [6,18], but doing this rigorously requires caution. If we simply compare $G(B)$ at a given V_{TG} before, between, and after illuminations, the disorder potential change is masked by an associated density-driven change in Fermi wavelength $\lambda_F \sim n^{-\frac{1}{2}}$ (for completeness, we nonetheless present this comparison in Fig. S2 of Ref. [32]); such a comparison is only meaningful at common n. To properly demonstrate the illumination-induced change in disorder potential we use the following procedure. First, we plot the gate sweeps to a transformed gate voltage axis $V'_{TG} = V_{TG} - V_{th}$ as shown in Fig. 2(a). The three traces have a common gradient but different fluctuation patterns such that the traces cross each other at various points. At these crossing points the device has the same $G(B = 0)$ and n for a given V'_{TG} before, between, and after the two illuminations, providing the most fair basis for comparing the corresponding $G(B)$ traces. One such instance is highlighted by the arrow at $V'_{TG} = +0.90$ V in the panel inset to Fig. 2(a); the three corresponding $G(B)$ traces

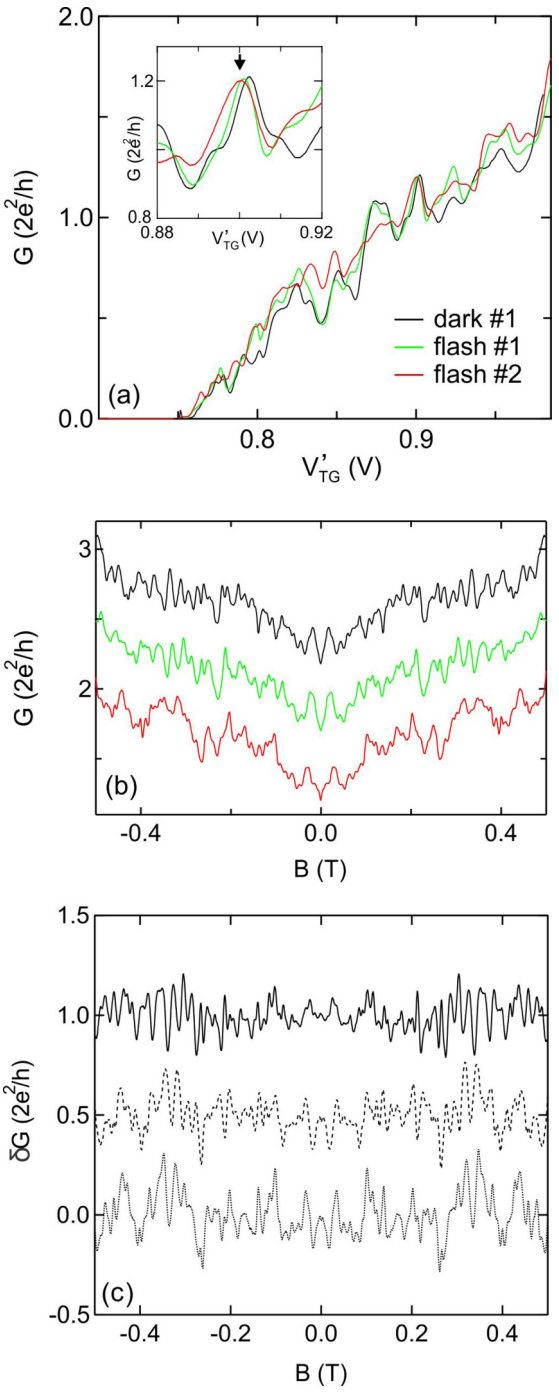

FIG. 2. (Color online) (a) Comparison of G vs transformed top gate voltage $V'_{TG} = V_{TG} - V_{th}$ where $V_{th} = 0{,}55{,}130$ mV for the dark #1 (black), flash #1 (green) and flash #2 (red) traces, respectively, using data from Fig. 1(a). (Inset) A magnified view of the main panel centered at $V'_{TG} = 0.90$ V showing a crossing point for the three traces as indicated by the arrow. (b) Dark #1, flash #1, and flash #2G vs B traces obtained at $V_{TG} = 0.900$ V (black), 0.845 V (green), and 0.770 V (red) corresponding to $V'_{TG} = 0.90$ V. (c) The MCF difference $\delta G = G(B)_{flash\#1} - G(B)_{dark\#1}$ (solid), $G(B)_{flash\#2} - G(B)_{flash\#1}$ (dashed), or $G(B)_{flash\#2} - G(B)_{dark\#1}$ (dotted) vs B highlighting the $G(B)$ changes resulting from illumination. In (b) and (c) the bottom trace is unshifted; remaining traces are sequentially offset upwards by $0.5 \times 2e^2/h$ for clarity.

are plotted in Fig. 2(b). The $G(B)$ traces vary significantly confirming a change in the dot's disorder potential [6,18]. This is highlighted in Fig. 2(c), where we plot the difference $\delta G = G(B)_{flash\#1} - G(B)_{dark\#1}$ (solid), $G(B)_{flash\#2} - G(B)_{flash\#1}$ (dashed), or $G(B)_{flash\#2} - G(B)_{dark\#1}$ (dotted) versus B. The latter highlights the cumulative change arising from the two illuminations. The cumulative rms fluctuation across the $0 < B < 0.5$ T range is 0.076, 0.088, and $0.108 \times 2e^2/h$, respectively. Each illumination causes an approximately equivalent change, but this effect ultimately diminishes due to the finite population of light-active centers; this typically occurs after four 100 ms illumination pulses for this device.

The most remarkable aspect of this device emerges in response to thermal cycling to room temperature. Figure 3(a) shows $G(B = 0)$ versus V_{TG} from the second cooldown before illumination, denoted dark #2 (solid), along with the corresponding trace from the first cooldown dark #1 (dashed). These two traces are essentially identical, as are $G(B)$ traces obtained at $V_{TG} = +0.9$ V [Fig. 3(b)]. Note that $V_{TG} = +0.9$ V is chosen out of convenience here; matching $G(B)$ for various V_{TG} were reported previously [18]. The $G(B)$ similarity is clear in the difference trace $\delta G(B) = G(B)_{dark\#2} - G(B)_{dark\#1}$ in Fig. 3(c), which is presented at matching scale to Fig. 2(c) for direct comparison. The cumulative rms fluctuation for the trace in Fig. 3(c) is $0.030 \times 2e^2/h$, a factor of 2–4 smaller than for the traces in Fig. 2(c). This indicates that the disorder potential returns to its initial configuration upon thermal cycling. In other words, in our undoped devices, illumination can be used to randomly reconfigure the disorder, and it can be "reset" to a repeatable base configuration by thermal cycling.

An interesting question is: What is the nature of the disorder enabling this ability to optically alter and then thermally reset the disorder potential? Two features of the data provide important clues. The first is that illumination increases the electron density [Fig. 1(b)], i.e., the sample displays persistent positive photoconductivity [35–37]. The second is that the impurity population returns to its initial ionization configuration after thermal cycling [Figs. 3(a) and 3(b)]. There are two possible impurity models (Fig. 4) that satisfy these features: Si background impurities acting as deep traps and C background impurities acting as shallow acceptors; it is highly likely both exist at different densities in our undoped heterostructures. We first address these individually with respect to persistent photoconductivity, before considering how they fit with our observation that we can reset the MCF, and thereby the disorder potential, to its initial configuration by room temperature thermal cycling.

A well known cause of persistent positive photoconductivity in $Al_xGa_{1-x}As$/GaAs heterostructures with $x > 0.2$ are deep-trapping Si DX centers in the AlGaAs layer [38,39]. Briefly, the Si DX center can take three possible states: shallow hydrogenic donor states d^0 and d^+, and a deep trap DX^- that is stabilized by lattice deformation [39,40]. The ground state is DX^- and it is exceptionally stable since the DX center ionization energy $\sim$100 meV [41] far exceeds the electron thermal energy at low temperature ($\sim$2.5 μeV at $T = 0.3$ K). However, the DX center can be optically excited to release one or both of its trapped electrons to become

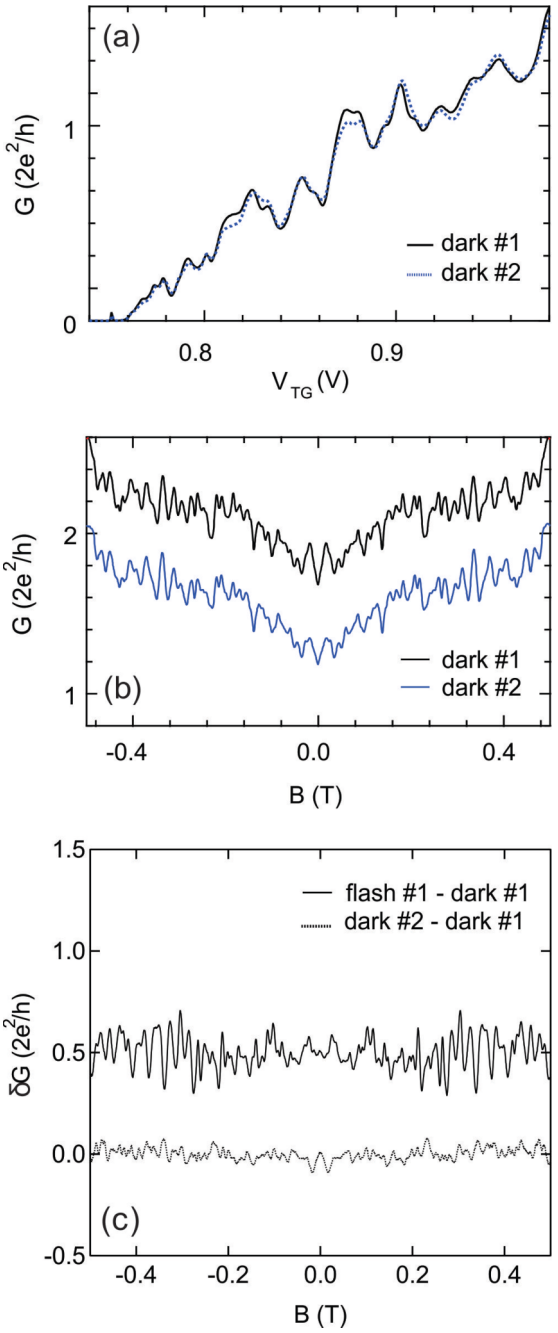

FIG. 3. (Color online) (a) Comparison of G vs V_{TG} obtained before illumination on the first cooldown, denoted dark #1 (black solid line), and after two illuminations and room temperature thermal cycling in the dark, denoted dark #2 (blue dashed line). (b) Comparison of G vs B at $V_{TG} = 0.9$ V for dark #1 (black) and dark #2 (blue); the dark #1 trace is offset vertically by $0.5 \times 2e^2/h$ for clarity. (c) The MCF difference $\delta G = G(B)_{dark\#2} - G(B)_{dark\#1}$ vs B (dashed) along with $\delta G = G(B)_{flash\#1} - G(B)_{dark\#1}$ vs B (solid) from Fig. 2(c) for comparison. The solid trace is offset upwards by $0.5 \times 2e^2/h$ for clarity.

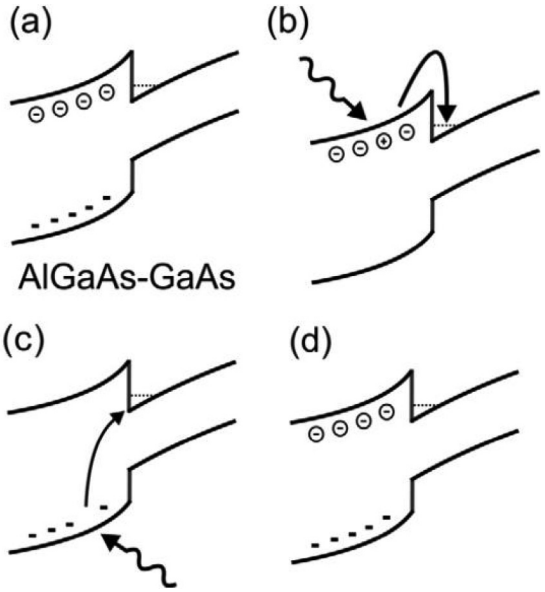

FIG. 4. Schematic band diagrams illustrating the two possible dopant-related mechanisms underpinning the "alter and reset" behavior observed in our device. As discussed in the text, the device initializes into a state (a) where all Si impurities are in the DX^- state (near CB in AlGaAs) and all C impurities are in the a^- state (near VB, only shown in AlGaAs, but also possible in GaAs layers). Optical illumination can excite electrons to the 2DEG (dashed line at GaAs side of AlGaAs-GaAs interface) via two processes: (b) $DX^- \rightarrow d^+$ [41], and (c) $a^- \rightarrow a^0$ [47]. The process $DX^- \rightarrow d^+$ cannot be achieved by electron thermal energy alone ($\sim$2.5 μeV at $T = 0.3$ K) since it is much less than the DX ionization energy $\sim$100 meV [41]; illumination is essential to these processes. The optically liberated electrons remain trapped in the 2DEG while the device remains at low temperature $T \lesssim 100$ K, with the associated ionized donors contributing to a varied disorder potential, as realized by the MCF measurements (Figs. 2/3). The device can be reset to its initial configuration (d) by room temperature thermal cycling.

d^0 or d^+ [40,41]. The latter is the ultimate outcome either way, as the transition $d^0 \rightarrow d^+$ requires much less energy than $DX^- \rightarrow d^0$ [41]. The optically liberated electrons either join the 2DEG [Fig. 4(b)] or are swept into the n^+ cap by the gate electric field. Note that these liberated electrons cannot be retrapped by Si impurities unless the sample is warmed above 100 K due to a lattice-deformation-induced energy barrier surrounding these impurities [38]. Thus an associated change in the charge between gate and 2DEG occurs, producing a negative shift in V_{th}, and equivalently, an increase in n at fixed V_{TG}, i.e., persistent photoconductivity. The presence of Si background impurities in our device is a logical possibility because a) the 2DEG is immediately adjacent to a 160 nm undoped $Al_xGa_{1-x}As$ layer with $x > 0.2$ and b) the MBE chamber contains a Si source for degenerate doping of the GaAs cap in these structures and modulation doping of other heterostructures grown during the same chamber evacuation. Ge, S, Se, Sn, and Te impurities can also produce deep-trapping DX centers in AlGaAs [38,42]; in particular, S is a common impurity in As MBE sources [43,44] and is proposed to also show DX behavior in GaAs [45,46]. Note that Si is a shallow hydrogenic donor in GaAs with states d^0 and d^+ only.

C background impurities are also common in MBE-grown AlGaAs/GaAs heterostructures [43,44]. Carbon is not known to show DX behavior [38], acting instead as a shallow acceptor

[47]. However, an ionized C acceptor a^- may be neutralized to a^0 by hole capture from a nearby photo-generated electron-hole pair. This electron-hole pair generation should occur, particularly in our GaAs layers, since we use a red LED in this experiment [48]. This process should result in positive persistent photoconductivity provided the photo-generated electron enters the 2DEG or n^+-GaAs cap [Fig. 4(c)], rather than being captured to re-ionize the same acceptor. This is possible because, unlike the DX center, there is no lattice-deformation-induced barrier surrounding the C impurity. Illumination can decrease the two-dimensional hole gas density in C-doped AlGaAs/GaAs heterostructures [49], presumably via a similar mechanism. One advantage of this model is that it is viable for both the undoped AlGaAs spacer and the GaAs substrate, unlike the Si DX center model discussed above.

We now turn our attention to the ability to reset the disorder potential and MCF to the initial, pre-illumination configuration by room temperature thermal cycling [Fig. 4(d)]. The fact that we observe this means that upon cooldown all impurities return to their initial charge states. In the simplest case, this implies: a) all acceptors, e.g., C impurities, are in the ionized a^- state, b) all donors, e.g., Si, S, etc. in GaAs are in the d^+ state, and c) all donors, e.g., Si, S, etc. in the AlGaAs are in the DX^- state. While this ignores some exotic possibilities, e.g., impurity complexes, these are likely rare due to the very low impurity density. We now consider the plausibility of this full ionization scenario. As a shallow acceptor, C in GaAs commonly shows electrical activation efficiencies well above 80% [47], with 100% activation found for doping densities less than 3×10^{17} cm^{-3} [50]. Activation is enhanced in $Al_xGa_{1-x}As$, increasing with Al content x [47]. We also expect full ionization of Si shallow donors in GaAs as their activation energy is 6 meV, compared to 26 meV for C shallow acceptors [51]. Complete Si activation is indeed observed at low doping densities [52]; autocompensation due to Si dopant amphotericity [53] and more complex donor deactivation mechanisms [54] only become important for Si densities above 10^{19} cm^{-3}. The return of all Si impurities in the AlGaAs to the DX^- state is the most unexpected outcome because in modulation-doped devices this does not occur [6,40]. However, the intentional Si density in modulation-doped structures is 1000–2000× greater than the background impurity density in our undoped heterostructures [55], even if we assume that all of the background impurities are Si, which is highly unlikely. In this instance, the free electron density in the AlGaAs during cooldown may sufficiently exceed the Si impurity density to doubly occupy all DX centers—there may be two coinciding mechanisms that aid this process.

The first is the tendency for background impurities, particularly Si, to ride upwards on the AlGaAs growth front [56,57]. This would push the bulk of the Si background impurities closer to the n^+-GaAs cap. The second is that the Fermi energy is pinned against the conduction band edge in the n^+-GaAs cap, which raises the local Fermi level in the upper parts of the AlGaAs spacer (e.g., see Fig. 2 of Ref. [58]). This should enhance the free electron density in the AlGaAs layer, increasing the probability for Si background impurities to take the DX^- state. Additionally, the lower Si background impurity density would increase the impurity spacing by a factor of at least 10 relative to modulation-doped heterostructures. This large spacing $\gtrsim 65$ nm should dramatically reduce charge migration between adjacent DX centers (i.e., $DX^- + d^+ \rightarrow d^+ + DX^-$), further enhancing MCF stability. It should also prevent charge migration between acceptor sites, and the associated slow drift in $G(B)$ recently reported for hole quantum dots [23].

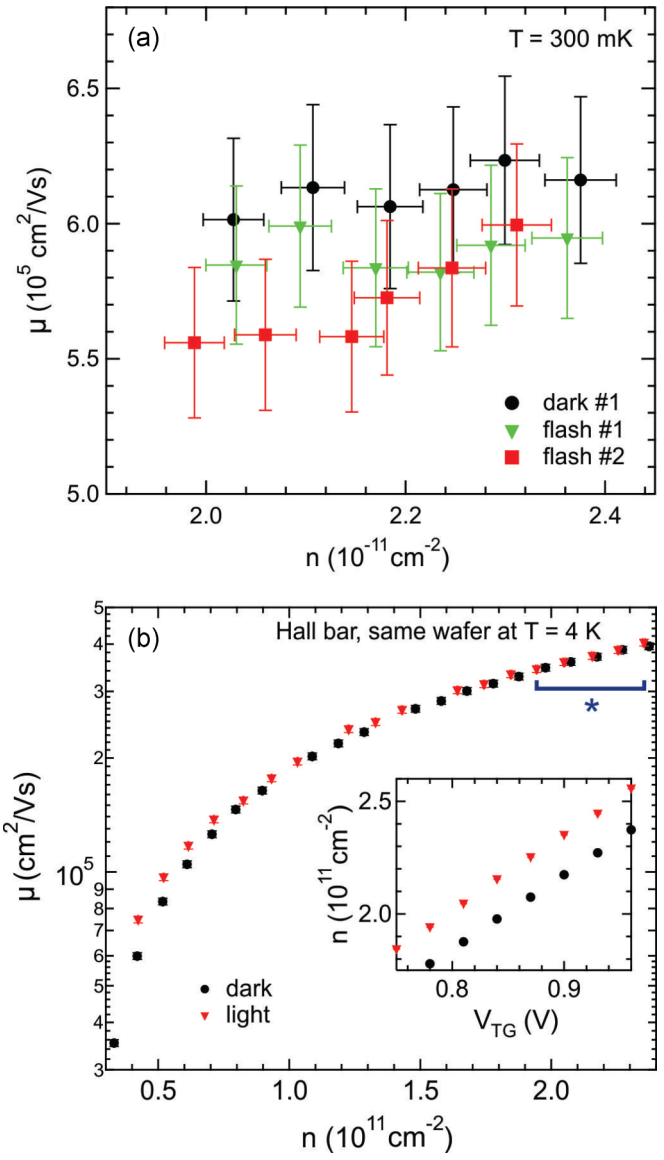

FIG. 5. (Color online) (a) The mobility μ vs electron density n for dark #1 (black circles), flash #1 (green triangles), and flash #2 (red squares) measured from Shubnikov-de Haas oscillations measured on a Hall-bar segment immediately adjacent to the quantum dot used to obtain data in Figs. 1–3. Data was obtained at $T = 300$ mK from a region of the Hall bar adjacent to the quantum dot. (b) The mobility μ vs electron density n obtained before (black circles) and after illumination (red triangles) measured for a separate Hall-bar sample made using the same heterostructure. Only the error bars in $\mu \sim 2\%$ are shown; the error bars in $n \sim 0.2\%$. The data was obtained at $T = 4$ K and the blue bracket marked $*$ indicates the operating density range for our quantum dot sample [cf. Fig. 1(b)]. Inset shows n vs top-gate voltage V_{TG} for this Hall bar for comparison with data from the quantum dot sample in Fig. 1(b).

We finish by briefly considering how this scenario fits with other transport properties. We previously reported a study of the ratio of the transport scattering lifetime τ_t to quantum scattering lifetime τ_q for the undoped wafer used here [55]. This ratio gives some idea of the proximity of ionized impurities to the 2DEG; the closer these impurities are, the smaller the ratio τ_t/τ_q [59]. We obtained $\tau_t/\tau_q \sim 10$ [55], which is consistent with the bulk of the ionized impurities being well separated from the 2DEG. Note that the "surface riding" mechanism discussed earlier for Si should also drive C impurities upwards in the AlGaAs layer [60].

Turning to the mobility, the transition $a^- \rightarrow a^0$ should result in a mobility increase as it eliminates a charged scattering center. In contrast, there should be little change in the mobility from the transition $DX^- \rightarrow d^+$ because negative DX^- centers and positive d^+ donors both cause Coulomb scattering of electrons in the 2DEG. This argument ignores DX center correlation effects [40], which might be justified given the $\sim 10\times$ higher donor separation; but for completeness, were there any correlations the random nature of DX center photoionization should reduce them, causing μ to decrease slightly [40]. Figure 5(a) shows μ vs n obtained Shubnikov-de Haas measurements from a Hall bar segment immediately adjacent to the quantum dot used for Figs. 1–3. This data suggests that $\mu(n)$ decreases with illumination, but the trend is barely significant relative to measurement error. In Fig. 5(b) we present characterization data for a separate Hall bar from the same heterostructure without any etched quantum dot. Here we observe an increase in $\mu(n)$ with illumination, which ranges from over 20% at low n to almost zero at high $n > 2 \times 10^{15}$ cm^{-2} where our device is operated (indicated by the blue $*$ in Fig. 5(b)). A similar increase in $\mu(n)$ was reported for undoped AlGaAs/GaAs heterostructures by Saku *et al.* [33], but their increase was larger, decreasing from $\sim$46% at $n \sim 2 \times 10^{10}$ cm^{-2} to $\sim$25% at $n \sim 2 \times 10^{11}$ cm^{-2}. Given the lack of a clear shift in μ with illumination in our operating n range, we suspect that *both* mechanisms $a^- \rightarrow a^0$ and $DX^- \rightarrow d^+$ are at play in our device, perhaps with the $a^- \rightarrow a^0$ process being slightly dominant. This is perhaps not surprising as there is no reason to expect that either Si or C cannot be present as background impurities. As a final note, one additional possibility that we acknowledge is extrinsic sources of defects in the Schottky barriers and etched surfaces nearby the active regions of our devices (e.g., surface states, oxides). We have no evidence that these play a role in the optically induced "alter and reset" behavior we report in our quantum dots here, but we suspect they are responsible for a gradual evolution of the MCF observed over longer time periods (i.e., weeks) when the devices are at room temperature, and particularly when stored in air. We cannot rule out that these extrinsic defects may have a small effect in larger undoped devices. Additional studies using custom-doped heterostructures and/or allied analytical methods, e.g., deep level transient spectroscopy (DLTS) [61], may assist in further understanding the underlying dopant photoexcitation processes involved in the device behavior we report. It may also be possible to distinguish the different charging mechanisms by varying the excitation photon energy from below to above the band-gap energy; this would be another interesting avenue for further research.

In summary, we have shown the ability to alter the disorder potential in undoped heterostructures by optical illumination, and then reset the disorder potential back to its initial configuration by thermally cycling the device to room temperature. Our data suggests that this process likely arises from a mixture of two processes: a) photoexcitation of ionized C background acceptors back to their neutral state, and b) photoionization of Si DX centers. This remarkable "alter and reset" capability is not possible in conventional modulation-doped heterostructures [6]. Our approach offers a route to studying how even small densities of optically-active charged background impurities influence transport in nanoscale devices. It could also be readily extended to the optimization of semiconductor materials for applications where extremely low disorder/scattering is vital to operation, e.g., quantum information processing [8,12]. Since the method only requires a quantum dot showing quantum interference fluctuations, the approach should also be transferrable to materials beyond III-V semiconductors, e.g., graphene [29,30].

This work was funded by the Australian Research Council (ARC). A.P.M. acknowledges an ARC Future Fellowship and A.R.H. acknowledges an ARC Outstanding Researcher Award. We thank L. Eaves, D. J. Carrad and S. P. Bremner for helpful discussions. This work was performed in part using the NSW node of the Australian National Fabrication Facility (ANFF).

[1] M. Y. Simmons, Nat. Phys. **4**, 165 (2008).
[2] X. Hu and S. Das Sarma, Phys. Rev. Lett. **96**, 100501 (2006).
[3] K. D. Petersson, J. R. Petta, H. Lu, and A. C. Gossard, Phys. Rev. Lett. **105**, 246804 (2010).
[4] Ç. Kurdak, C.-J. Chen, D. C. Tsui, L. Parihar, S. Lyon, and G. W. Weimann, Phys. Rev. B **56**, 9813 (1997).
[5] Q.-Z. Yang, M. J. Kelly, I. Farrer, H. E. Beere, and G. A. C. Jones, Appl. Phys. Lett. **94**, 033502 (2009).
[6] B. C. Scannell, I. Pilgrim, A. M. See, R. D. Montgomery, P. K. Morse, M. S. Fairbanks, C. A. Marlow, H. Linke, I. Farrer, D. A. Ritchie, A. R. Hamilton, A. P. Micolich, L. Eaves, and R. P. Taylor, Phys. Rev. B **85**, 195319 (2012).
[7] M. P. Jura, M. A. Topinka, L. Urban, A. Yazdani, H. Shtrikman, L. N. Pfeiffer, K. W. West, and D. Goldhaber-Gordon, Nat. Phys. **3**, 841 (2007).
[8] W. Pan, N. Masuhara, N. S. Sullivan, K. W. Baldwin, K. W. West, L. N. Pfeiffer, and D. C. Tsui, Phys. Rev. Lett. **106**, 206806 (2011).
[9] C. Nayak, S. H. Simon, A. Stern, M. Freedman, and S. Das Sarma, Rev. Mod. Phys. **80**, 1083 (2008).
[10] R. Dingle, H. L. Störmer, A. C. Gossard, and W. Wiegmann, Appl. Phys. Lett. **33**, 665 (1978).
[11] K.-J. Friedland, R. Hey, H. Kostial, R. Klann, and K. Ploog, Phys. Rev. Lett. **77**, 4616 (1996).

[12] V. Umansky, M. Heiblum, Y. Levinson, J. Smet, J. Nübler, and M. Dolev, J. Cryst. Growth **311**, 1658 (2009).
[13] Y. Hirayama, J. Appl. Phys. **80**, 588 (1996).
[14] R. H. Harrell, K. S. Pyshkin, M. Y. Simmons, D. A. Ritchie, C. J. B. Ford, G. A. C. Jones, and M. Pepper, Appl. Phys. Lett. **74**, 2328 (1999).
[15] P. M. Solomon, C. M. Knoedler, and S. L. Wright, IEEE Electron Device Lett. **5**, 379 (1984).
[16] B. E. Kane, L. N. Pfeiffer, K. W. West, and C. K. Harnett, Appl. Phys. Lett. **63**, 2132 (1993).
[17] W. R. Clarke, C. E. Yasin, A. R. Hamilton, A. P. Micolich, M. Y. Simmons, K. Muraki, and Y. Hirayama, Nat. Phys. **4**, 55 (2008).
[18] A. M. See, I. Pilgrim, B. C. Scannell, R. D. Montgomery, O. Klochan, A. M. Burke, M. Aagesen, P. E. Lindelof, I. Farrer, D. A. Ritchie, R. P. Taylor, A. R. Hamilton, and A. P. Micolich, Phys. Rev. Lett. **108**, 196807 (2012).
[19] A. P. Micolich, A. M. See, B. C. Scannell, C. A. Marlow, T. P. Martin, I. Pilgrim, A. R. Hamilton, H. Linke, and R. P. Taylor, Fortschr. Phys. **61**, 332 (2013).
[20] S. Feng, P. A. Lee, and A. D. Stone, Phys. Rev. Lett. **56**, 1960 (1986).
[21] C. M. Marcus, A. J. Rimberg, R. M. Westervelt, P. F. Hopkins, and A. C. Gossard, Phys. Rev. Lett. **69**, 506 (1992).
[22] Z.-L. Ji and K.-F. Berggren, Phys. Rev. B **52**, R11607 (1995).
[23] D. J. Carrad, A. M. Burke, O. Klochan, A. M. See, A. R. Hamilton, A. Rai, D. Reuter, A. D. Wieck, and A. P. Micolich, Phys. Rev. B **89**, 155313 (2014).
[24] S. Washburn and R. A. Webb, Rep. Prog. Phys. **55**, 1311 (1992).
[25] K. S. Ralls, W. J. Skocpol, L. D. Jackel, R. E. Howard, L. A. Fetter, R. W. Epworth, and D. M. Tennant, Phys. Rev. Lett. **52**, 228 (1984).
[26] W. J. Skocpol, P. M. Mankiewich, R. E. Howard, L. D. Jackel, D. M. Tennant, and A. D. Stone, Phys. Rev. Lett. **56**, 2865 (1986).
[27] G. P. Whittington, P. C. Main, L. Eaves, R. P. Taylor, S. Thoms, S. P. Beaumont, C. D. W. Wilkinson, C. R. Stanley, and J. Frost, Superlatt. Microstruct. **2**, 381 (1986).
[28] D. E. Beutler, T. L. Meisenheimer, and N. Giordano, Phys. Rev. Lett. **58**, 1240 (1987).
[29] N. E. Staley, C. P. Puls, and Y. Liu, Phys. Rev. B **77**, 155429 (2008).
[30] Y. Ujiie, S. Motooka, T. Morimoto, N. Aoki, D. K. Ferry, J. P. Bird, and Y. Ochiai, J. Phys.: Condens. Matter **21**, 382202 (2009).
[31] A. M. See, O. Klochan, A. R. Hamilton, A. P. Micolich, M. Aagesen, and P. E. Lindelof, Appl. Phys. Lett. **96**, 112104 (2010).
[32] See Supplemental Material at http://link.aps.org/supplemental/10.1103/PhysRevB.91.085417 for LED emission spectrum and additional magnetoconductance data.
[33] T. Saku, K. Muraki, and Y. Hirayama, Jpn. J. Appl. Phys. **37**, L765 (1998).
[34] J. P. Bird, R. Akis, D. K. Ferry, D. Vasileska, J. Cooper, Y. Aoyagi, and T. Sugano, Phys. Rev. Lett. **82**, 4691 (1999).
[35] H. L. Störmer, A. C. Gossard, W. Wiegmann, and K. Baldwin, Appl. Phys. Lett. **39**, 912 (1981).
[36] D. V. Lang and R. A. Logan, Phys. Rev. Lett. **39**, 635 (1977).
[37] R. J. Nelson, Appl. Phys. Lett. **31**, 351 (1977).
[38] D. V. Lang, R. A. Logan, and M. Jaros, Phys. Rev. B **19**, 1015 (1979).
[39] P. M. Mooney, J. Appl. Phys. **67**, R1 (1990).
[40] E. Buks, M. Heiblum, Y. Levinson, and H. Shtrikman, Semicond. Sci. Technol. **9**, 2031 (1994).
[41] P. M. Mooney, Semicond. Sci. Technol. **6**, B1 (1991).
[42] O. Kumagai, H. Kawai, Y. Mori, and K. Kaneko, Appl. Phys. Lett. **45**, 1322 (1984).
[43] B. J. Skromme, S. S. Bose, B. Lee, T. S. Low, T. R. Lepkowski, R. Y. DeJule, G. E. Stillman, and J. C. M. Hwang, J. Appl. Phys. **58**, 4685 (1985).
[44] E. C. Larkins, E. S. Hellman, D. G. Schlom, J. J. Harris, M. H. Kim, and G. E. Stillman, J. Cryst. Growth **81**, 344 (1987).
[45] C. H. Park and D. J. Chadi, Phys. Rev. B **54**, R14246 (1996).
[46] M.-H. Du and S. B. Zhang, Phys. Rev. B **72**, 075210 (2005).
[47] C. Giannini, C. Gerardi, L. Tapfer, A. Fischer, and K. H. Ploog, J. Appl. Phys. **74**, 77 (1993).
[48] R. Fletcher, E. Zaremba, M. D'Iorio, C. T. Foxon, and J. J. Harris, Phys. Rev. B **41**, 10649 (1990).
[49] C. Gerl, J. Bauer, and W. Wegscheider, J. Cryst. Growth **301-302**, 145 (2007).
[50] H. Ito, O. Nakajima, and T. Ishibashi, Appl. Phys. Lett. **62**, 2099 (1993).
[51] R. F. Pierret, *Advanced Semiconductor Fundamentals* (Prentice Hall, New York, 2002).
[52] E. F. Schubert, L. Pfeiffer, K. W. West, H. S. Luftman, and G. J. Zydzik, Appl. Phys. Lett. **64**, 2238 (1994).
[53] S. Schuppler, D. L. Adler, L. N. Pfeiffer, K. W. West, E. E. Chaban, and P. H. Citrin, Appl. Phys. Lett. **63**, 2357 (1993).
[54] C. Domke, Ph. Ebert, M. Heinrich and K. Urban, Phys. Rev. B **54**, 10288 (1996).
[55] S. J. MacLeod, K. Chan, T. P. Martin, A. R. Hamilton, A. See, A. P. Micolich, M. Aagesen, and P. E. Lindelof, Phys. Rev. B **80**, 035310 (2009).
[56] M. Heiblum, J. Vac. Sci. Technol. B **3**, 820 (1985).
[57] L. N. Pfeiffer, E. F. Schubert, K. W. West, and C. W. Magee, Appl. Phys. Lett. **58**, 2258 (1991).
[58] W. R. Clarke, A. P. Micolich, A. R. Hamilton, M. Y. Simmons, K. Muraki, and Y. Hirayama, J. Appl. Phys. **99**, 023707 (2006).
[59] B. Laikhtman, M. Heiblum, and U. Meirav, Appl. Phys. Lett. **57**, 1557 (1990).
[60] N. M. Cho, D. J. Kim, A. Madhukar, P. G. Newman, D. D. Smith, T. Aucoin, and G. J. Iafrate, Appl. Phys. Lett. **52**, 2037 (1988).
[61] D. V. Lang, J. Appl. Phys. **45**, 3023 (1974).